Sixth International Symposium on Turbulence and Shear Flow Phenomena
Seoul, Korea, 22-24 June 2009

LARGE EDDY SIMULATION OF FREE-STREAM TURBULENCE EFFECTS ON HEAT TRANSFER TO A HIGH PRESSURE TURBINE CASCADE

Rathakrishnan Bhaskaran
Department of Mechanical Engineering,
Stanford University
Stanford, CA, 94305, USA
rbhas@stanford.edu

Sanjiva K. Lele
Department of Mechanical Engineering and Aeronautics and Astronautics,
Stanford University
Stanford, CA, 94305, USA
lele@stanford.edu

ABSTRACT

Large Eddy Simulation (LES) of an uncooled, transonic, linear HP turbine vane cascade has been pursued using a high-order numerical method with about 83 million grid points. Heat transfer and aerodynamics of the blade is investigated in the presence of free-stream turbulence (FST). Quantitative comparisons with the experiments of Arts et al. (1990) show satisfactory agreement. The distortion of vortices from the inflow turbulence in the cascade passage leads to formation of long streamwise streaky structures, leading to transition of suction side boundary layer. Significant heat transfer augmentation is seen on both the pressure and suction sides due to the presense of these structures. Transition to turbulence, possibly due to streak instability and adverse pressure gradient effects is observed in the last 10% of the blade suction surface.

INTRODUCTION AND OBJECTIVES

The current trend in gas turbine engine design is to achieve better efficiency through higher turbine inlet temperature. As a result, the nozzle guide vanes and rotor blades of a high pressure (HP) turbine cascade are subject to an increasingly hostile thermal environment. High levels of turbulence and hot streaks from the upstream combustor impinge on the HP turbine blade rows. New, improved blade materials, and efficient cooling technology have sustained this rise in turbine inlet temperature. Heat transfer prediction of the thermally critical regions of a HP turbine has been a vital element in the design of gas turbine engines.

The primary focus of the current work is to investigate, using high fidelity numerical simulations, the effect of free-stream turbulence on the blade boundary layer and heat transfer augmentation in a high pressure turbine guide vane cascade. More complex phenomenon, such as rotor-stator interaction, discrete hole film-cooling, blade surface roughness effects, etc. are not considered in the present study. An uncooled, transonic, linear guide vane cascade designed at the von Kármán Institute (VKI) for fluid dynamics at Belgium by Arts et. al. (1990) is used as the model geometry. Heat transfer measurements for a wide range of experimental conditions were made at VKI. Inlet turbulence levels of $Tu\% \sim 1-6$, exit Reynolds number based on chord in the range of $Re \sim 500,000 - 2,000,000$ and exit Mach number of $Ma \sim 0.9 - 1.1$ was used in a short duration blow down facility to measure heat transfer to the vane.

NUMERICAL METHOD AND COMPUTATIONAL GRID

A high-order overset compressible Large Eddy Simulation (LES) procedure is used to numerically simulate the flow in this HP vane cascade. The compressible Navier-Stokes equations in conservation form are solved in a general curvilinear coordinate frame using dual implicit-explict time advancement scheme. The governing equations are:

$$\frac{\partial \rho}{\partial t} + (\rho v^k)_{,k} = 0, \quad (1)$$

$$\frac{\partial}{\partial t}(\rho v^i) + (\rho v^i v^j), j = -(g^{ij} p)_{,j} + \tau^{ij}_{,j}, \quad (2)$$

$$\frac{\partial E}{\partial t} + [(E+p)v^j]_{,j} = (\kappa g^{ij} T_{,i})_{,j} + (\tau^{ij} g_{ik} v^k)_{,j}, \quad (3)$$

where v^i, ρ, p, and T are the contravariant velocity components, density, pressure, and temperature respectively. The total energy E, and the viscous stress tensor τ^{ij} are given by

$$E = \frac{p}{\gamma - 1} + \frac{1}{2}\rho g_{ij} v^i v^j, \quad (4)$$

$$\tau^{ij} = \mu[g^{jk} v^i_{,k} + g^{ik} v^j_{,k} - \frac{2}{3} g^{ij} v^k_{,k}]. \quad (5)$$

g_{ij} and g^{ij} are the covariant and contravariant metric tensors respectively. The subscript $()_{,j}$ denotes covariant derivative. In writing the above equations, the Einstein summation convention is used (an index repeated once in the subscript and superscript of any term is summed over).

The physical velocity components are non-dimensionalized by the free-stream speed of sound c_∞, the density by the free-stream density ρ_∞, the pressure by $\gamma \rho_\infty c_\infty^2$ and the temperature by $(\gamma - 1)T_\infty$. This set of equations is closed by the equation of state

$$p = \frac{\gamma - 1}{\gamma} \rho T \quad (6)$$

The equations for the LES are obtained by applying a low pass filter on the above set of governing equations. The resulting subgrid scale fluxes are closed by using a dynamic

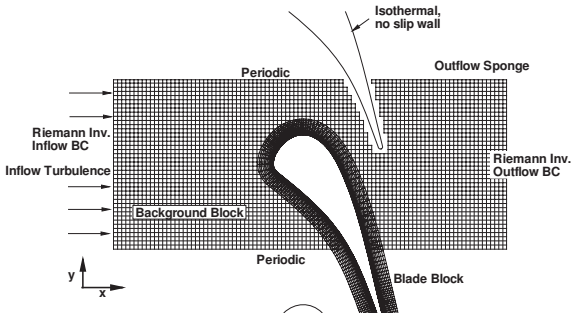

Figure 1: The grid used for the LES, along with the boundary conditions. Only every tenth grid point is shown for clarity.

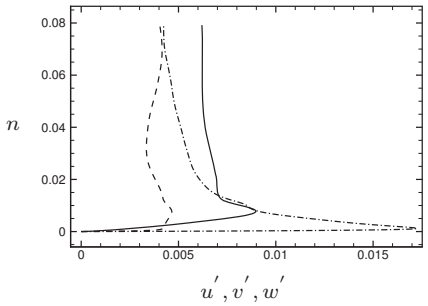

Figure 2: Development of velocity fluctuation along the stagnation streamline. The solid line is the streamwise component, dashed line is the transverse component and the dash-dotted line is the spanwise component of the fluctuation velocity.

procedure. A sixth-order compact scheme for spatial discretization with a staggered arrangement of variabales is used. A mixed second order implicit scheme with approximate factorization and a third order explicit Runge-Kutta scheme is used for time advancement. See Nagarajan et. al. (2003) for the details.

A fourth order Hermite interpolation scheme (Delfs 2001) is used for exchange of information between the grid blocks. In two dimensions, the Hermite interpolation at an overlap point is constructed using the function values and the first derivatives at the four surrounding points which bound the interpolated point in the uniform computational space. A local grid system (ξ, η) is constructed in the computational space, with the origin of the coordinate system at the center of the box formed by the points bounding the interpolated point. The coordinates of the interpolated point in this local coordinate system are found by the inverse mapping $(\xi, \eta) = M^{-1}(x, y)$. The forward mapping $M(\xi, \eta)$ is defined at all points using the Hermite interpolation scheme, and the inverse mapping $M^{-1}(x, y)$ is found using a Newton-Raphson procedure. The interpolation formula is given by

$$\begin{aligned} f(\xi,\eta) \quad = \quad & \sum_{l,k=0}^{1} C^0_{lk}(\xi,\eta) f_{i+l,j+k} + \\ & C^\xi_{lk}(\xi,\eta) \left[\frac{\partial f}{\partial \xi}\right]_{i+l,j+k} + \\ & C^\eta_{lk}(\xi,\eta) \left[\frac{\partial f}{\partial \eta}\right]_{i+l,j+k} + O(\Delta^4) \end{aligned} \qquad (7)$$

where C^0_{lk}, C^ξ_{lk}, and C^η_{lk} are the coefficients of interpolation. The details of the implementation can be found in Delfs (2001).

The primary geometrical properties of the blade are: chord of 67.647 mm, pitch to chord ratio of 0.85, stagger angle of 55 degrees (measured from the axial direction) and leading edge diameter to chord ratio of 0.122. A spanwise box of size 0.17 was used for the computation. A body-fitted O-grid block of size $1600 \times 201 \times 160$ which is advanced in time using an implicit scheme is used around the blade to resolve the boundary layer. This O-grid block is embedded in a background H-grid block of size $960 \times 408 \times 80$, which is advanced in time using an explicit time advancement scheme and is used to provide good resolution for the incoming turbulence. A schematic of the grid used in the simulation and the boundary conditions are shown in Figure 1. Isothermal, no-slip boundary conditions are applied at the walls of the balde. Characteristic boundary conditions based on Riemann invariants are applied at the inflow and outflow plane. A damping sponge is also applied near the outflow boundary to supress spurious acoustic reflections. Periodic boundary conditions are applied in the y-direction on the background grid in order to simuilate an infinite cascade of blades. Periodic boundary conditions are also applied in the spanwise direction.

Precomputed boxes of turbulence (Xiong et. al., 2004) with a desired turbulence intensity are passed into the domain through the inflow boundary (Bhaskaran & Lele, 2008).

RESULTS AND DISCUSSION

A LES simulation matching flow conditions from the experimental data set MUR226 has been performed. The key parameters of this data set are: Reynolds number based on the inlet velocity and chord of 134,580, inlet Mach number of 0.15, exit Mach number of 0.92, ratio of blade wall temperature to total inlet temperature of 0.75 and ratio of outlet to total inlet presure of 0.578. The inflow turbulence intensity is specified to be $Tu\% = 4$ in the data set, but other characteristics of the turbulence such as its length scale or spectra have not been reported.

Precomputed turbulence supplied at the inflow boundary of the computational box is simply convected by the mean flow with almost zero strain rate until about a distance of a quarter of chord from the blade leading edge when the stretching and tilting process due to the rapidly straining flow near the blade leading edge distorts the turbulence. The straining is primarily inviscid until inside the boundary layer, leading to large enhancement of the spanwise velocity fluctuation (Figure 2) as predicted by Rapid Distortion Theory (RDT). All three components of turbulence are ultimately suppressed in the boundary layer.

Time averaged wall statistics

Data from the simulation was colected for a duration of time when the inlet mean flow had moved by about five chords. Time and spanwise averaged isentropic Mach number distribution from the LES on the surface of the blade is plotted in Figure 3. Arts et. al. (1990) did not measure blade pressure distribution for the flow conditions of this simulation case, but the isentropic Mach number distribution from a closely related case MUR45 is shown as symbols

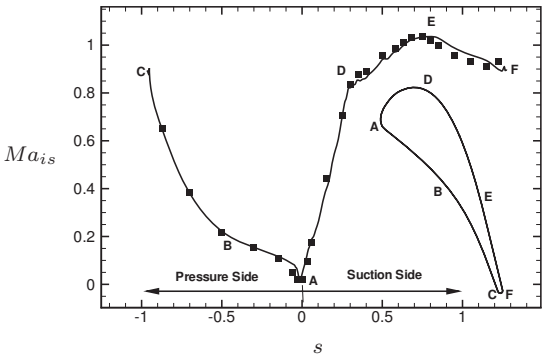

Figure 3: Isentropic Mach number distribution on the surface of the blade. Symbols are from Arts (1990) experimental data set MUR45, and the line is the present LES matching conditions of MUR226. Various sections of the curve and their corresponding stations on the blade surface are marked.

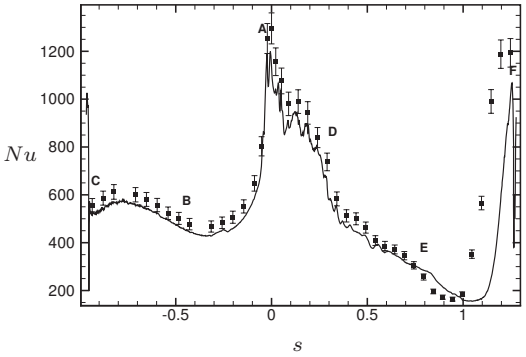

Figure 4: Nusselt number distribution on the surface of the blade. Symbols are from Arts (1990) experimental data set MUR226, and the line is the present LES simulation matching flow conditions of MUR226.

in the figure. The good agreement between the simulation and experiement shows that the LES has captured the overall blade pressure distribution well.

The flow sees a favorable pressure gradient on all of the pressure side. The pressure gradient is gradual between A-B and then becomes large in B-C. The flow sees a favorable pressure gradient through most of the suction side also; the flow accelerates from A-E followed by a slight adverse pressure gradient zone between E-F. These structures in the boundary layer in these different zones are quite different, and will be described in a later section.

Time and spanwise average hear transfer distribution is shown in the blade Nusselt number plot in Figure 4. The overall shape of the blade heat transfer profile is quite well captures by the LES, but the heat transfer coefficient is slightly underpredicted. Also the boundary layer seems to be transition later on the suction side as compared with the experiments. A possible explantion of this behavior could be the mismatch in the length scale of the turbulence that was specified at the inflow plane in the LES. It has been shown using simulaions with organized spanwise disturbances by Xiong & Lele (2004) that leading edge heat transfer coefficient is quite sensitive not only to the amplitude of the turbulence, but also to its length scale. A larger length

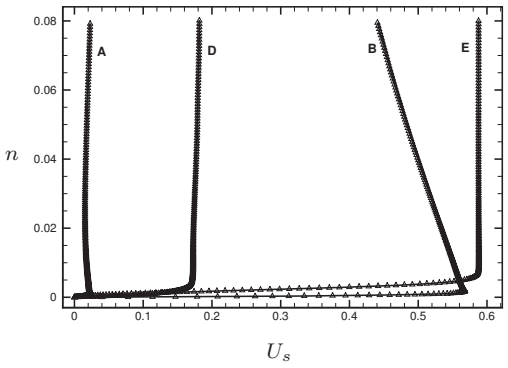

Figure 5: Mean tangential (s) velocity profile at stations A, B, D and E.

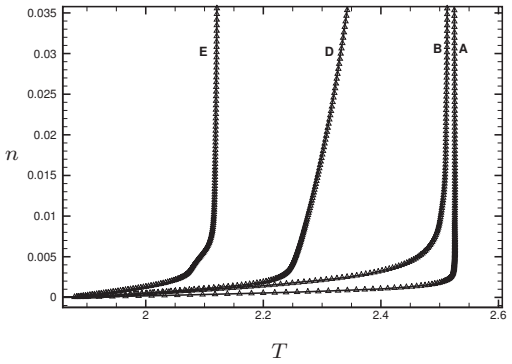

Figure 6: Mean temperature profile at stations A, B, D and E.

scale turbulence was found to produce lesser heat tranfer augmentation, while a higher intensity turbulence was observed to cause greater heat transfer augmentation. A major limitation of Arts et. al.'s experimental data set is the characterization of the inflow turbulence. Turbulence intensity at only one station (at the inflow plane) is reported. They do not report the length scale or dissipation rate of the turbulence, or the intensity at any other station. Pecnik and Sanz (2007) have performed RANS simulations of this blade configuration and have reported (through private communication) that heat transfer and location of transition was sensitive to the turbulence dissipation rate at the inflow plane in their RANS model. Simulations with organized spanwise inflow disturbance similar to Xiong & Lele (2004) are being performed for this blade configuration in order to access the importance of the disturbance length scale on heat transfer.

The time averaged streamwise (s) component of velocity and mean temperature are shown in Figures 5 – 6 at stations A, B, D and E along the pressure and suction sides of the blade. The mean velocity and thermal boundary layer profiles are well resolved at these stations.

Near wall grid resolution

Near wall grid resolution requirements are similar to that of a DNS in order to capture the boundary layer instability process leading to transiton and accurate prediction of heat transfer. Only the suction side boundary layer shows transition at this Reynolds number. The near wall grid spacing

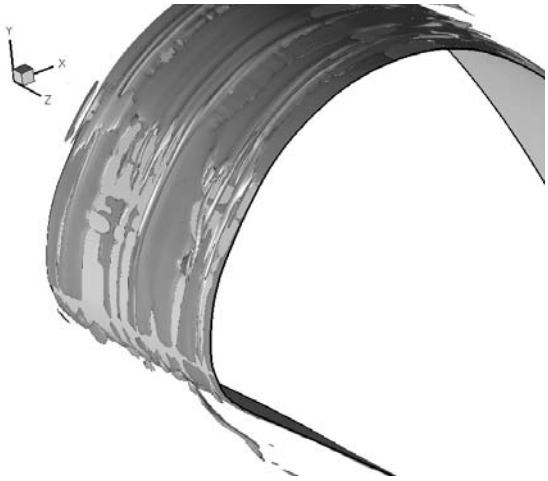

Figure 7: Iso-surfaces of λ_2 show intense stretching of vortices from the inflow turbulence around the leading edge.

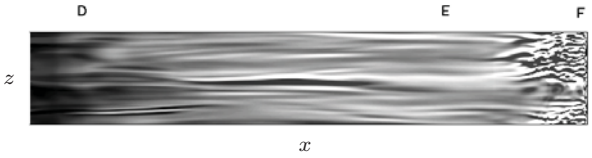

Figure 8: x-vorticity on the suction side showing breakdown of streaks in to turbulence.

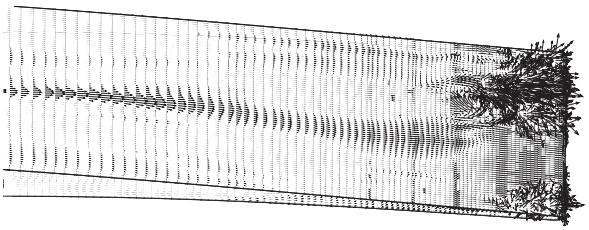

Figure 9: Fluctuation velocity vectors on the suction side boundary layer show meandering low and high velocity fluid streaks.

based on the local wall shear velocity in the transition zone E-F on the suctions side in the streamwise (s), wall-normal (n) and spanwise (z) directions were about 30, 1 and 20 respectively. The boundary layer remains laminar over most of the suction side from A to E and all of the pressure side, where the long streaky structures in the boundary layer need to be sufficiently resolved.

Structures in the boundary layer

Eddies from the inflow turbulence are stretched around the leading edge (Figure 7), leading to significant enhancement of local streamwise (s) vorticity near the leading edge. The penetration of these vortices in the thermal boundary layer near the leading edge cause significant enhancement in heat transfer (Xiong et. al., 2007).

These streamwise oriented vortices wrap around the leading edge and are transported in to the favorable pressure gradient zone (D-E) on the suction side boundary layer forming long streamwise streaky structures (Figure 8). The spanwise scale of these structures is much smaller than the streamwise scale. These structures appear to grow downstream both in amplitude and dimension, leading to formation of turbulent patches in the adverse pressure gradient zone (E-F). Figure 9 shows fluctuation velocity vectors (time and spanwise mean velocity subtracted) inside the suction side boundary layer. Regions of positive and negative fluctuation velocity vectors help visualize the meandering of regions of low and high speed fluid in these long streaky structures. A zoomed in view of the region E-F in Figure 10 show a large high speed streak in the middle of the domain, which slows down in the adverse pressure gradient zone E-F to form a large low speed zone near the trailing edge region. Visualization using iso-surfaces of λ_2 (the second largest eigenvalue of $S^2 + \Omega^2$, Jeong & Hussain, 1995) show the presense of a large streamwise oriented vortex in zone E-F (Figure 11) at this instant. The boundary layer stays laminar in the vicinity of this vortex. There seems to be a good correlation between the location of the streaks and the presence of turbulent spots, indicating a streak instability mechanism could be active.

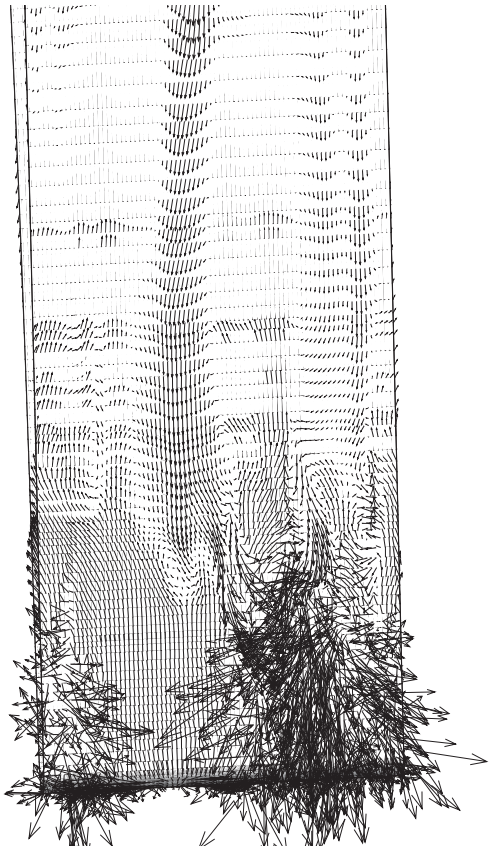

Figure 10: The boundary layer in zone EF remains laminar in the large streak in the middle of the domain on the suction side.

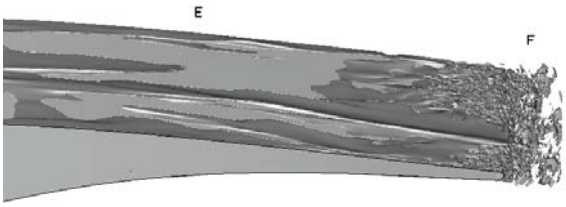

Figure 11: Iso-surfaces of λ_2 show that the boundary layer stays laminar in the region of the large vortex in the middle of the blade in zone E-F.

The streaks break down to form Λ shaped turbulent spots (Figure 12), probably under the influence of multiple insta-

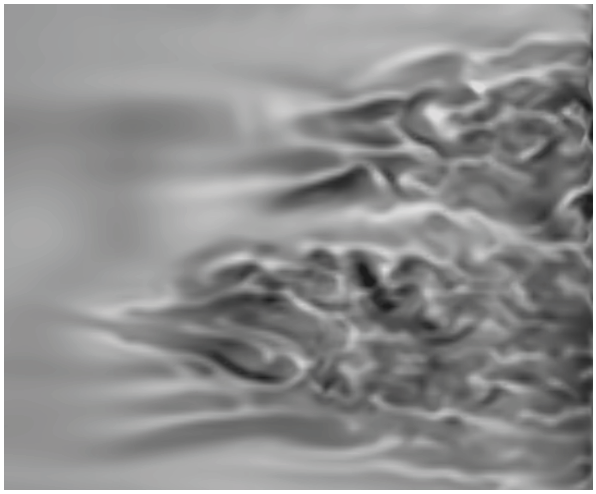

Figure 12: Λ shaped turbulent spots are seen on the suction side boundary layer in zone E-F in these contours of density.

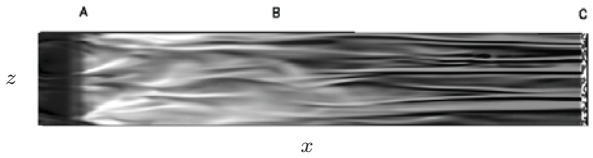

Figure 13: x-vorticity on the pressure side show long streamwise streaks. The structures in the mildly favorable pressure gradient zone A-B is are very different from the strongly favorable pressure gradient zone B-C.

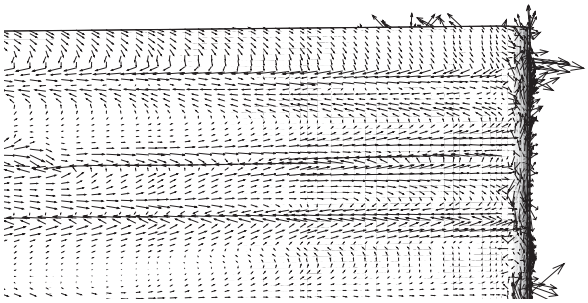

Figure 14: Flucutation velocity vectors on the pressure side boundary layer show Görtler type alternating regions of low and high speed streaks.

bility mechanism. Depending on the amplitude and length scale of inflow turbulence, a combination of streak instability, adverse pressure gradient in zone E-F or T-S wave mechanism could be the cause for appearance of turbulent spots (Alfredsson & Matsubara, 1996).

The structures on the pressure side boundary layer are quite different. The vortices from the inflow turbulence appear to form meandering snake like structures (Figure 13) in zone A-B, where there is a very mild favorable pressure gradient. Their spanwise dimension is comparable to the streamwise dimension. They however appear to align along the streamwise direction, forming long streaky structures in the strongly favorable pressure gradient zone B-C. Regions of alternating sign streamwise vorticity appears to be Görtler type vortices.

These streaky structures perturb the temermal boundary layer, causing enhancement in heat tranfer. Fluctuation velocity vectors in Figure 15 and fluctuation temperature

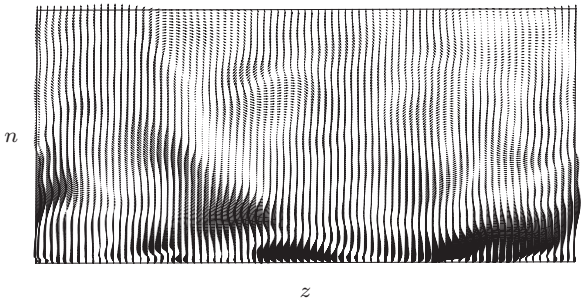

Figure 15: Fluctuation velocity vectors in a plane normal to the pressure side near point B.

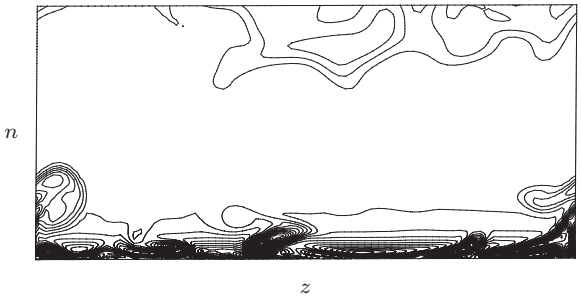

Figure 16: Temperature fluctuation contours at the same location as Figure 15 show that the thermal boundary layer is perturbed due to the streaky structures.

contours in Figure 16 show that the streaky structures lead to formation of unsteady mushroom like thermal structures in the boundary layer, similar to that seen by Xiong & Lele (2007). The streamwise oriented vortices transport hot fluid away and towards the wall according to the direction of the local fluid velocity in the vortex being away or towards the wall, thus creating regions of low and high heat transfer respectively.

CONCLUSIONS

The effect of inflow free-stream turbulence on the heat transfer and boundary layer stability on a high pressure turbine vane has been studied using a high-fidelity numerical simulation procedure. Good comparison with the experiments of Arts et. al. (1990) of blade isentropic Mach number distribution and heat transfer has been observed. Preliminary numerical visualization of the boundary layer flow has shown presence of long streamwise streaky structures on both the suction and pressure sides of the blade. Multiple instability mechanisms appear to be operational, leading to transition of the suction side boundary layer. Further simulations with varying amplitude and length scale inflow turbulence will help in better understading the blade heat transfer augmentation and boundary layer instability mechanisms.

ACKNOWLEDGMENTS

R. Bhaskaran would like to thank Dr. S. Nagarajan for his technical assistance during the development of the overset LES solver based on a code he had originally developed. The authors would like to thank Dr. E. van der Weide for providing the code used for the RANS simulation to generate initial conditions for the LES. Helpful discussions with Dr. R. Pecnik on interpretation of results from his RANS

simulations of the VKI HP vane cascade and with Prof. G. Iaccarino on mesh generation are greatfully acknowledged. The Air Force Office of Scientific Research (AFOSR) has provided partial sponsorship for this work. Computational resources provided by the Army Research Laboratory (ARL) is gratefully appreciated.

REFERENCES

Alfredsson, P.H., and Matsubara, M., "Streaky structures in transition," *Transitional Boundary Layers in Aeronautics*, pp. 374–386, Elsevier, 1996.

Arts, T., Lambert de Rouvroit, M., and Rutherford, A.W., "Aero-Thermal investigation of a highly loaded transonic linear turbine guide vane cascade," *Technical Note 174*, von Kármán Institute for Fluid Dynamics, Belgium, 1990.

Bhaskaran, R., and Lele, S.K., "Development of Large Eddy Simulation for Aero-Thermal Prediction in High Pressure Turbine Cascade," *AIAA Paper*, 2008-4146-924, 2008.

Delfs, J.W., "An overlapped grid technique for high resolution CAA schemes for complex geometries," *AIAA paper*, 2001-2199, 2001.

Jeong, J., and Hussain, F., "On the identification of a vortex," *J. of Fluid Mechanics*, Vol. 285, 1995, pp. 69–94.

Nagarajan, S., Lele, S.K., and Ferziger, J.H., "A robust high-order compact method forlarge eddy simulation," *J. Computational Physics*, Vol. 191, 2003, pp. 392–419.

Pecnik, R., and Sanz, W., "Application of the turbulent potential model to heat transfer prediction on a turbine guide vane," *J. of Turbomachinery*, Vol. 129, 2007, pp. 628–635.

Xiong Z., and Lele, S.K., "Distortion of upstream disturbances in a Hiemenz boundary layer," *J. of Fluid Mechanics*, Vol. 519, 2004, pp. 201–232.

Xiong Z., and Lele, S.K., "Stagnation point flow and heat transfer under free stream turbulence," *J. of Fluid Mechanics*, Vol. 590, 2007, pp. 1–33.

Xiong Z., Nagarajan, S. and Lele, S. K., "A simple method for generating inflow turbulence," *AIAA J.*, Vol. 42, No. 10, 2004, pp. 2164–2166.